Scientific Journal for Damietta Faculty of Science **15**(2) 2025, 226-236
Doi: 10.21608/sjdfs.2025.394223.1238
ISSN Print 2314-8594
ISSN Online 2314-8616

https://sjdfs.journals.ekb.eg/

Comparative Analysis of Spectral Indices to Assess Coastal Salinization in Northeastern Nile Delta, Egypt

Reem A. ElNaggar*[1], Ayman I. Taha[2], Hany M. Shaaban[2], Eman R. Nofal[3] and Hatem M. Aboelkhair[1]

[1]Faculty of Science Damietta University, 34517, Damietta, Egypt.
[2]National Research Institution for astronomy and geophysics, 11722, Helwan, Cairo, Egypt.
[3]Research Institute for Groundwater, National Water Research Center, 13621, El-Kanater El-Khairiya, Egypt.

Received: 14 June 2025 /Accepted: 22 June 2025

*Corresponding author's E-mail: reem.elnaggar@du.edu.eg

Abstract

Soil salinization driven by seawater intrusion poses a growing threat to agriculture in the northeastern Nile Delta, where shallow groundwater tables and intensive irrigation facilitate salt accumulation at the surface. This study mapped surface salinity and its impact on vegetation along a 50 km area from New Mansoura City to Mansoura using a Landsat 8 OLI. Unsupervised K-means clustering identified five land-use/land-cover classes (water, vegetation, barren land, urban, and sabkha), allowing for the computation of eight spectral indices per class: Normalized Difference Vegetation Index (NDVI), Soil-Adjusted Vegetation Index (SAVI), Salinity Indices S1–S4, Normalized Difference Salinity Index (NDSI), and Vegetation Soil Salinity Index (VSSI). Zonal statistics quantified index distributions, and linear regression of index values against distance from the shoreline assessed spatial trends. Vegetation indices (NDVI, SAVI) effectively highlighted canopy stress but showed minimal coastal gradients ($\beta_1 \approx -1.8 \times 10^{-6}$ m^{-1}; $R^2 \approx 0$), reflecting the mitigating effect of local irrigation. Brightness-based indices and NDSI captured salt-crust signatures, with mean S1–S3 values increasing from agricultural fields (13 222–14 972) to sabkha (19 122–20 080) and positive but low-magnitude coastal slopes (e.g., S1 $\beta_1 = 0.1255$ m^{-1}; $R^2 < 0.003$). The hybrid VSSI provided the strongest separation between vegetated and salt-stressed zones (mean VSSI: –79 163 vs. –125 610). These results demonstrate differential sensitivity of spectral indices to salinity and vegetation stress, which can be used to monitor soil salinity with minimum cost and apply further analysis and surveys only when necessary.

Keywords: Soil salinity, Seawater intrusion, Landsat 8, Remote sensing, salinity monitoring

Introduction

Soil salinization from seawater intrusion is a growing threat to coastal agriculture worldwide. Rising sea levels and reduced river flows are allowing saltwater to penetrate farther inland, increasing soil salt content and harming crops (Bear, 1999). In Egypt's Nile Delta – one of the world's most vulnerable deltas – sea levels have been rising, pushing saltwater into soils and

aquifers and leading to higher soil salinity. Persistent irrigation practices combined with seasonal fluctuations in the water table have led to widespread salt accumulation, compromising soil structure, reducing agricultural productivity, and degrading ecosystem health (Armanuos et al., 2022; Nofal et al., 2015).

Human activity in this region is intensive. The Dakahlia governorate is a major agricultural area where farms grow rice, cotton, wheat and high-value vegetables and fruits, many of which are irrigated from the Nile's Damietta Branch and local aquifers (Alshrabsy et al., 2024; Mansour & Mark, 2025). New Mansoura is a planned coastal city developed for housing and industry. The local economy also includes agro-industry and export-oriented horticulture. This heavy water use, combined with low elevation and rising sea levels, has worsened waterlogging and salt intrusion. Sea-level rise and reduced flow in the Damietta branch are causing brackish water to invade croplands and aquifers, leading to soil degradation and deteriorated vegetation. Protecting this fertile delta requires reliable monitoring of salinity levels.

Remote sensing techniques offer a cost-effective and spatially comprehensive approach for monitoring surface salinity over large areas, overcoming the limitations of sparse in-situ measurements (Nguyen et al., 2020). Researchers have developed numerous spectral indices that correlate with soil salt content or with vegetation stress resulting from salinity (Table 1). Common indices include the Normalized Difference Vegetation Index (NDVI) and Soil-Adjusted Vegetation Index (SAVI), which drops as salt stress reduces plant greenness; Normalized Difference Salinity Index (NDSI) and various Salinity Indices (S1–S4) that are designed to highlight bare soils with high salt reflectance; and specialized indices like the Vegetation Soil Salinity Index (VSSI), which combines visible/infrared bands to detect salt under partial vegetation cover. Many studies have shown strong correlations between these indices and measured soil electrical conductivity (EC) in field surveys (Dehni & Lounis, 2012).

These spectral indices have been successfully applied in coastal and delta regions worldwide. In Vietnam's Mekong Delta (Tra Vinh Province), (Nguyen et al., 2020) used Landsat 8 to compute NDVI, SAVI, VSSI and other indices and found that the near-infrared band and the VSSI had the strongest correlation with measured soil salinity ($R^2 \approx 0.80$ and 0.70, respectively). Their Landsat-derived salinity maps (for the topsoil) agreed closely with in-situ EC measurements, demonstrating that satellite data can reliably track coastal salinity intrusion. In Pakistan's Indus Delta, (Aeman et al., 2023) linked saltwater-driven changes in vegetation to electrical conductivity using the VSSI: areas undergoing erosion and intrusion showed high VSSI values (0.7–1.2) and elevated EC, whereas accreting regions had lower VSSI and more mangrove growth. Other studies in arid and semi-arid deltas have reported similar results using multi-temporal Landsat analyses (using NDSI, BI, SI, NDVI, SAVI, etc.) and have mapped salinity variations in Turkish coastal plains (Azabdaftari & Sunar, 2016).

The main objective of this study is to assess the effectiveness of spectral indices derived from Landsat-8 in detecting and mapping surface soil salinity along a 50 km stretch between New Mansoura and Mansoura. By evaluating how well these indices reflect actual salinity patterns in a region undergoing rapid environmental and anthropogenic changes, we aim to identify reliable remote sensing indicators for monitoring salinity intrusion.

We hypothesize that vegetation- and soil-based spectral indices, particularly VSSI and NDSI, will show strong spatial correspondence with observed salinity gradients in this part of the Nile Delta, due to their sensitivity to both bare soil reflectance and vegetation stress. The findings could guide improved land management, crop planning, and salinity mitigation efforts to sustain agriculture and the local economy in the face of environmental stress.

Table 1 Spectral indices employed for evaluating vegetation condition and soil salinity in the study area. Each index is defined by its mathematical expression and associated reference, with formulations designed to enhance sensitivity to either vegetation vigor or surface salt accumulation

Index	Equation	Reference
SAVI	$SAVI = ((1 + L) * NIR - Red)/(Red + NIR + L)$	(Huete, 1988)
NDVI	$NDVI = {NIR - Red}/{NIR + Red}$	(Khan et al., 2001)
NDSI	$NDSI = (NIR - Red)/(NIR + Red)$	(Khan et al., 2001)
S1	$S1 = \sqrt{Green^2 + Red^2}$	(Douaoui et al., 2006)
S2	$S2 = \sqrt{Red * Green}$	(Douaoui et al., 2006)
S3	$S3 = \sqrt{Blue * Red}$	(Khan et al., 2001)
S4	$S4 = \sqrt{Green^2 + Red^2 + NIR^2}$	(Douaoui et al., 2006)
VSSI	$VSSI = 2 * Green - 5 * (Red + NIR)$	(Dehni & Lounis, 2012)

Study area

The study area is situated along a 50 km southeastward profile in the northeastern Nile Delta, extending from the northwestern margin of New Mansoura City to Mansoura (Figure 1). It is a flat, low-lying coastal plain formed by Nile sediments and shaped by Mediterranean marine influences. Geomorphologically, the area comprises a narrow coastal belt of dunes and sand flats, backed by a fluvio-marine plain and an inland floodplain (Pennington et al., 2017). Near the coast, the soil is predominantly sandy (fine sand) with low organic matter, while the soil on the former river delta platforms is medium- to fine-textured loams and clays (El Nahry et al., 2015). In the Mansoura area, recent studies have recorded extreme salinization (soil EC up to ~190 dS/m) in some fields, attributed to shallow saline groundwater and seawater intrusion (Youssef et al., 2024).

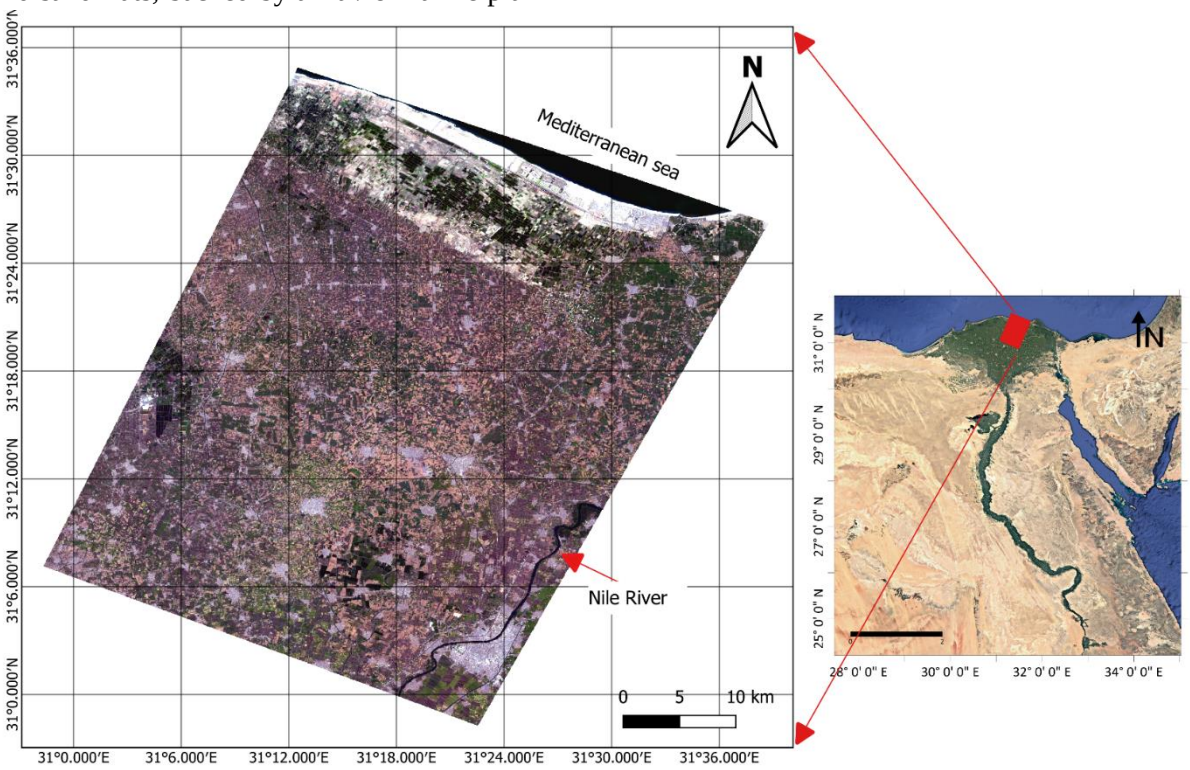

Figure 1: True Color satellite image showing the study area located in the northern part of the east and middle delta within the jurisdiction of Damietta and Dakahlia Governates.

Methodology

This study combined geospatial processing in QGIS 3.28 with quantitative analysis in Python to characterize surface salinity and its impact on vegetation in a coastal zone subject to seawater intrusion. A Level-2T Landsat 8 OLI image (September 2022) was selected for salinity assessment based on local climatic conditions. As shown in the climate (Figure 2), September corresponds to a period of minimal precipitation and moderate temperatures. This combination is ideal for analyzing salinity using spectral indices, as it minimizes surface moisture interference that could obscure the spectral signature of salt crusts and stressed vegetation. Indices such as NDSI, SI, and VSSI are more effective under drier conditions, where reflectance from salt-affected soils and stressed vegetation is clearer and more distinguishable. Additionally, avoiding months of peak summer temperatures (e.g., July and August) helps reduce the confounding effects of thermal stress on vegetation, which could mimic or mask salinity symptoms. Therefore, the September image offers an optimal balance, with low moisture and moderate temperature conditions that enhance the reliability of salinity index detection in coastal environments prone to seawater intrusion.

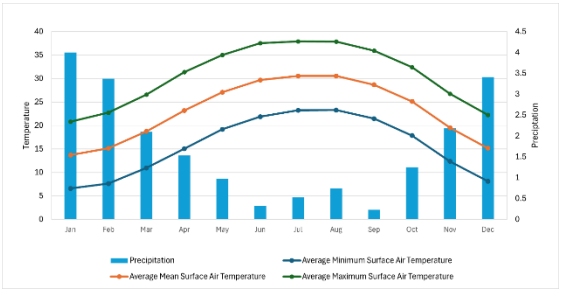

Figure 2 : Monthly Climatology of Average of Minimum Surface Air Temperature, Average Mean Surface Air Temperature, Average Maximum Surface Air, Temperature & Precipitation 1991-2020; Arab Republic of Egypt

Eight spectral indices (NDVI, SAVI, NDSI, S1–S4, VSSI) were calculated via the Raster Calculator tool in QGIS software (Table 1). Employing the unsupervised K-means LULC classification, we obtained 5 classes: water, vegetation, barren, urban, and sabkha classes (Figure 3). In Python, a Pearson correlation matrix was calculated with pandas to assess interrelationships among indices (Abdi, 2007). Subsequently, ordinary least squares (OLS) linear regression models were used to evaluate how each index varied with coastal distance, yielding slope, intercept, $\mathscr{R}^2$, and p-values for each LULC class. This integrated workflow ensured reproducible spatial and statistical analysis of salinity trends and vegetation stress.

Spectral indices

Landsat 8's Operational Land Imager (OLI) provides multispectral data at 30 m resolution across visible, near-infrared (NIR), and shortwave-infrared (SWIR) bands, enabling the computation of spectral indices that exploit contrasts in soil brightness and vegetation stress associated with salinization (Cao et al., 2022). A Level-2 T Landsat 8 OLI image processed for atmospheric and geometric correction by Landsat, acquired on 09 September 2022, was obtained from the USGS Earth Explorer archive, including bands 2 (Blue) through 7 (SWIR). No additional temporal images or in situ salinity measurements were available; instead, index performance was validated through comparison with established results from the literature.

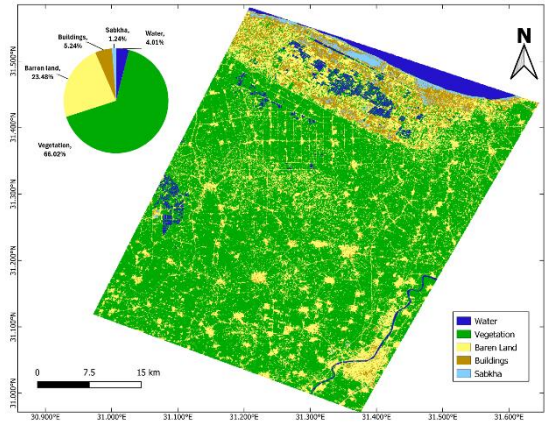

Figure 3 LULC map of the study area with class proportions. Vegetation is dominant, while sabkha and water cover minimal areas, derived from K-mean classification of Landsat 9 image

Normalized Difference Vegetation Index (NDVI).

Although originally developed for crop-health assessment, NDVI serves as an indirect salinity indicator in semi-arid and arid environments (Table 1), since high soil salinity induces plant stress and canopy thinning, which lowers NIR reflectance relative to red. Thus, declines in NDVI can signal zones of elevated surface

salinity where vegetation is adversely affected (Figure 4).

Soil-Adjusted Vegetation Index (SAVI).

To correct for soil-background brightness in sparse vegetation, SAVI modifies NDVI by introducing a canopy-density factor (L) (Table 1). This adjustment reduces soil-line influence, particularly important in semi-arid sabkha fringes, yielding improved detection of vegetation stress due to salinity. Compared to NDVI, SAVI offers greater sensitivity to salinity-induced canopy changes in areas of low to moderate vegetation cover (Huete, 1988) (Figure 4).

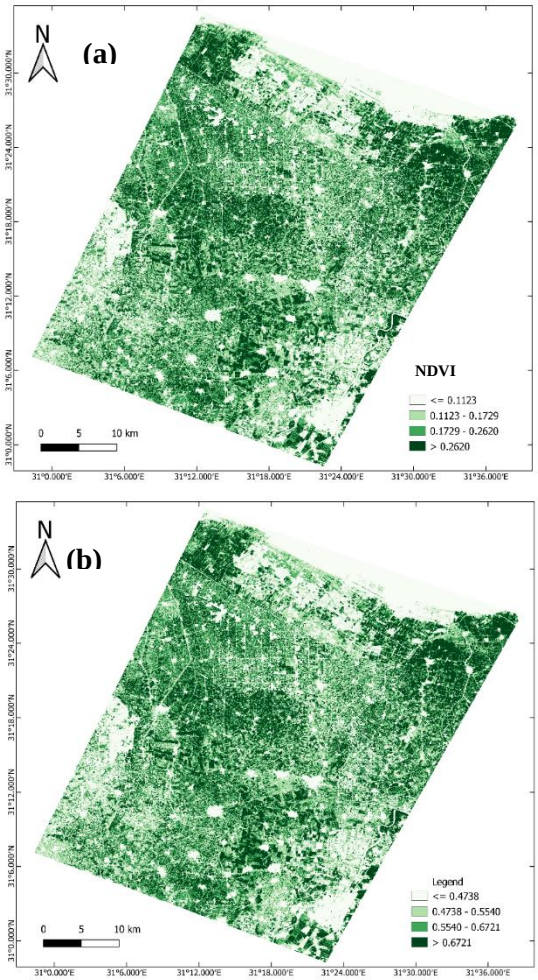

Figure 4 (a) Normalized Difference Vegetation Index (NDVI) map highlighting vegetation density; lower values indicate stressed or sparse vegetation. (b) Soil-Adjusted Vegetation Index (SAVI) map showing no difference in detection in sparsely vegetated areas through soil brightness correction.

Normalized Difference Salinity Index (NDSI).

Saline soil often exhibits higher reflectance in the red region (due to salt crusts and soil brightness) and lower reflectance in the NIR. By inverting the NDVI formulation (Table 1), NDSI directly targets salt-encrusted surfaces, producing high values in sabkha and salt-affected zones. Its simplicity and sensitivity to surface salts make it a widely used index in deltaic salinity studies (Figure 5).

Brightness-Based Indices (S1, S2, S3, S4).

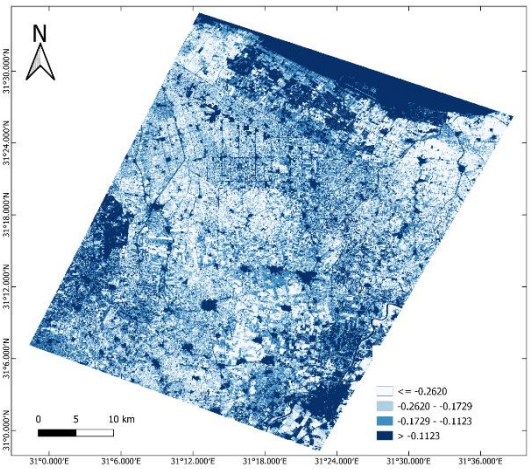

Figure 5 Normalized Difference Salinity Index (NDSI) map identifying salt-affected zones; higher values correspond to increased salinity presence.

Salt-affected soils typically exhibit high reflectance across visible bands, producing elevated S1–S4 values (Table 1). The S1–S4 indices were employed to quantify soil brightness and surface reflectance characteristics associated with salinity. S1 captures overall soil brightness by combining the red and green bands using a Euclidean norm, assigning higher values to bright or salt-encrusted soils and lower va' $_{SA}$ to darker, organic-rich surfaces. Although it may face limitations in sandy terrain, S1 is particularly effective in the silty, dark soils typical of the Nile Delta. S2 quantifies brightness as a geometric mean of red and green reflectance, offering a more balanced sensitivity to vegetated and non-vegetated areas, though it may be influenced by mixed land covers. S3 emphasizes reflectance in the blue and red bands, enhancing detection of salt crusts that strongly reflect in these wavelengths. S4 integrates green, red, and NIR reflectance into a composite brightness index. However, its

reliance on the NIR band can reduce its effectiveness in areas with minimal vegetation, especially where salinity obscures spectral vegetation signals (Figure 6).

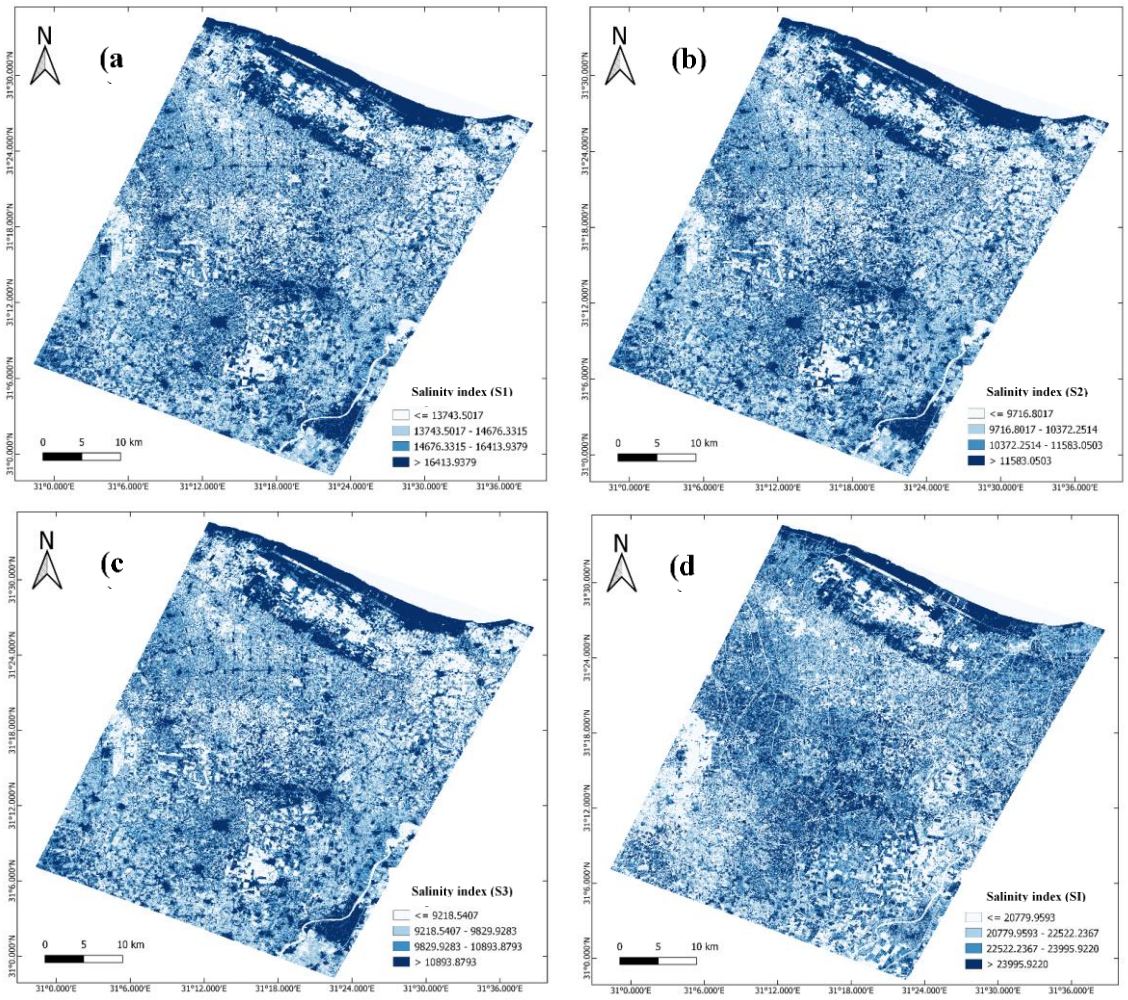

Figure 6 (a) S1 index map capturing soil brightness variations linked to salt crust formation, with lighter areas indicating higher salinity.(b) S2 index map showing enhanced spectral sensitivity to saline soils, useful in detecting sabkha and salt flats.(c) S3 index map highlighting subtle salt-induced brightness changes in coastal soils, aiding in delineation of salinized zones. (d) Salinity Index (S4) map reflecting soil salinity levels based on visible and near-infrared reflectance, with brighter regions suggesting salt accumulation.

Vegetation–Soil Salinity Index (VSSI).

Proposed by (Dehni & Lounis, 2012), the VSSI integrates spectral responses from both vegetation and bare-soil bands to discriminate between vegetation stress and pure soil brightness Table (1). High negative VSSI values correspond to stressed vegetation over saline soils, whereas less negative values mark healthy vegetation or non-saline soils. In practice, VSSI enhances separation of sabkha from vegetated areas under mixed-cover conditions, improving mapping accuracy along ecotonal transitions Figure (7).

All spectral indices—namely NDVI, NDSI, SI, S1, S2, S3, VSSI, and SAVI—were computed from a single Landsat 8 Operational Land Imager (OLI) scene acquired in September 2022. Each index was calculated according to its specific spectral formula and saved as a separate raster layer for subsequent analysis. To analyze the spatial trends of salinity indicators, zonal statistics were extracted based on land use/land cover (LULC) classifications derived via unsupervised K-means clustering. This step enabled the computation of mean, minimum, maximum, and standard deviation values for each index within each classified LULC zone. These zonal summaries provided the basis for understanding how salinity-related reflectance patterns varied across different surface types and their spatial relationship to coastal proximity.

The statistical component of the analysis was

conducted in Python (version 3.10), leveraging the libraries pandas, numpy, and rasterio and linregress linear regression from SciPy library for data manipulation and linear regression modeling. For each spectral index, a simple linear regression model was constructed to examine the trend of reflectance values as a function of distance from the coast. This approach was applied independently to each LULC class to account for land cover variability.

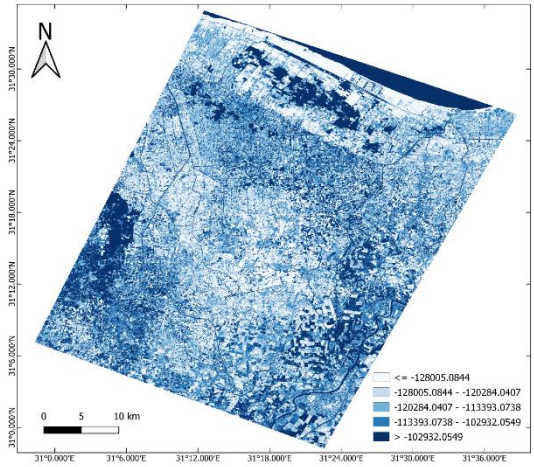

Figure 7 Vegetation–Soil Salinity Index (VSSI) map integrating vegetation and soil responses to effectively distinguish salinity-affected ecotones.

The coefficient of determination ($\mathscr{R}^2$) was used for model performance and o determine the significance of the regression slope (p-value). A statistically significant negative or positive slope was interpreted as a potential indicator of increasing or decreasing salinity gradients, respectively, which may be linked to seawater intrusion. The use of linear regression in this context provides a quantifiable measure of spatial salinity trends, building upon its established application in environmental remote sensing (Montgomery, 2013). By integrating QGIS-based spatial processing with Python's robust statistical framework, the methodology ensured a reproducible, transparent, and scalable workflow for coastal salinity assessment.

Results

This study evaluated the performance of multiple spectral indices in detecting coastal salinization and differentiating saline-affected surfaces, particularly sabkhas, from vegetated areas. Emphasis was placed on the ability of brightness- and salinity-related indices to capture both absolute salinity and spatial gradients from the shoreline inland.

Land-Use/Land-Cover Distribution

The unsupervised K-means clustering produced a clear delineation of five land-use/land-cover (LULC) classes across the 50 km profile (Table 2). Vegetation dominates the study area, covering 66.05 % (1,618 km²), followed by barren land at 23.70 % (575 km²). Water bodies, urban areas, and sabkha account for the remaining 4 % (98 km²), 5 % (129 km²), and 1 % (30 km²), respectively. This distribution reflects the intensive agricultural use of the Nile Delta's fluvial plains, interspersed with salt-flat (sabkha) patches near the coast and expanding urban development in the study area.

Table 2: LULC class area statistics along the study area.

Class	Pixel Count	Area (km²)	Percentage (%)
Water	109 309	98.38	4.00
Vegetation	1 798 179	1 618.36	66.05
Barren land	639 383	575.44	23.70
Urban	142 816	128.53	5.32
Sabkha	33 794	30.41	1.19

Vegetation-Based Indices: NDVI and SAVI

The Normalized Difference Vegetation Index (NDVI) and Soil-Adjusted Vegetation Index (SAVI) both decline markedly in areas affected by salinity stress, yet their sensitivity differs by land cover. In the vegetation class, NDVI values range from –0.105 to 0.530 (mean = 0.200, SD = 0.087), whereas barren land exhibits slightly lower vegetation signals (mean = 0.185, SD = 0.098). Sabkha areas show near-zero NDVI (mean = 0.067, SD = 0.066), reflecting minimal healthy vegetation (Table 3). SAVI amplifies these differences by compensating for low canopy cover: vegetation areas yield a mean SAVI of 0.330 (SD = 0.143), barren land 0.306 (SD = 0.161), and sabkha only 0.111 (SD = 0.109).

Linear regression of NDVI against distance from the shoreline produced a slight negative slope ($\beta_1 = -1.83\times10^{-6}$ m^{-1}; $p < 0.001$), though R^2 was effectively zero, indicating that coastal proximity exerts only a weak influence on canopy greenness across the transect. SAVI regression mirrored this trend ($\beta_1 = -1.83\times10^{-6}$

m^{-1}; $p < 0.001$), confirming that soil-adjustment does not substantially alter the spatial gradient in vegetation stress under these conditions. These results suggest that while NDVI and SAVI effectively distinguish salinity-impacted vegetation in mixed-cover zones, their spatial trends are muted by irrigation and crop management practices that mitigate coastal salinity effects.

Table 3: NDVI and SAVI statistics by LULC class.

Index	Class	Mean	SD	Min	Max
NDVI	Vegetation	0.2000	0.0869	–0.1051	0.5299
	Barren	0.1852	0.0976	–0.1268	0.5541
	Sabkha	0.0673	0.0662	–0.1168	0.4331
SAVI	Vegetation	0.3300	0.1434	–0.1733	0.8743
	Barren	0.3056	0.1610	–0.2092	0.9142
	Sabkha	0.1110	0.1093	–0.1928	0.7147

Salinity-Specific Indices: NDSI and Brightness Metrics

The Normalized Difference Salinity Index (NDSI) and brightness-based indices (S1, S2, S3, S4, and SI) exhibited stronger sensitivity to soil salinity than vegetation-based indices. Mean NDSI values were consistently negative, reflecting higher SWIR reflectance relative to NIR—a pattern indicative of salinity presence. Among the land cover classes, sabkha areas recorded the highest (least negative) NDSI values (mean = –0.067), followed by water (–0.042) and vegetation (–0.200), consistent with surface salt accumulation. However, linear regression of NDSI against distance from the shoreline produced negligible slopes ($\beta_1 \approx 0$; $R^2 < 0.01$) (Table 4), suggesting limited capability to capture subtle salinity gradients across mixed land cover and moisture conditions.

Brightness-based indices displayed clearer differentiation among land cover classes. The S1 index showed the strongest contrast, with mean values increasing from 13,222 in vegetated areas to 19,122 in sabkha, accompanied by a moderate standard deviation. This suggests good class separation with limited internal variation, making S1 the most effective indicator of surface salinity under the study area conditions. S2 and S3 indices exhibited similar spatial trends, although S2 may be more sensitive to mixed land covers or transition zones. All three indices showed positive but low-magnitude regression slopes (e.g., S1: $\beta_1 = 0.1255$ m^{-1}, $p < 0.001$; $R^2 < 0.003$) (Table 4), suggesting slightly increased soil brightness near the coast.

In contrast, the S4 index displayed high standard deviation across all classes, indicating substantial internal variability and potential class overlap. Its reliance on the near-infrared (NIR) band may reduce its reliability in highly reflective or mixed-cover environments, consistent with (Douaoui et al., 2006) findings. These results collectively highlight the superiority of the S1 index in detecting surface salinity and differentiating between stressed sabkha and vegetated lands. While indices like NDSI and S2 remain informative, their performance is more susceptible to land cover complexity and soil moisture variability.

Table 4 NDSI and brightness-based index statistics by LULC class.

Index	Class	Mean	SD	Min	Max
NDSI	Vegetation	–0.2000	0.0869	–0.5299	0.1051
	Sabkha	–0.0673	0.0662	–0.4331	0.1168
S1	Sabkha	19 122.40	4 131.03	11 351.48	34 287.72
	Vegetation	13 222.02	2 549.09	9 528.08	30 010.39
S2	Sabkha	13 488.49	2 904.09	8 013.29	24 152.97
	Vegetation	9 334.83	1 799.21	6 737.05	21 188.67
S3	Sabkha	12 509.92	2 503.71	7 666.96	22 256.57
	Vegetation	8 841.66	1 596.32	3 103.01	19 020.99
S4	Sabkha	25 157.34	5 633.83	13 596.55	45 909.51
	Vegetation	16 929.69	4 266.71	13 115.99	37 970.43

Vegetation–Soil Salinity Index (VSSI)

The Vegetation–Soil Salinity Index (VSSI) exhibits strong class discrimination, with mean values ranging from –79 163 in vegetation to –125 610 in sabkha. More negative VSSI indicates greater vegetation stress over saline soils (Table 5). Despite this clear separation, VSSI's regression slope is effectively zero across all classes, reflecting uniform salinity stress within each LULC category rather than a linear coastal gradient. Nevertheless, VSSI's ability to integrate vegetation and soil reflectance makes it a powerful tool for mapping mixed-cover salinity impacts, especially in ecotonal zones where pure soil or vegetation indices may fail.

Table 5: VSSI statistics by LULC class

Class	Mean	SD	Min	Max
Water	-79163.38	26226.418	-195647	0.5299
Vegetation	-115531.06	14321.255	-215576.25	0.5541
Barren land	-116886.53	14902.781	-242398.83	0.4331
Urban	-122518.195	18939.1	-228510.69	
Sabkha	-125609.83	31828.773	-235678.62	

Correlation matrix

The correlation matrix of the spectral indices revealed distinct interrelationships that underscore their utility in monitoring soil

salinity and vegetation status (Figure 8). Strong positive correlations were observed between vegetation-based indices, particularly the Normalized Difference Vegetation Index (NDVI) and Soil-Adjusted Vegetation Index (SAVI), which showed a perfect correlation (r = 1.00). This reflects their similar mathematical structure and consistent response to green biomass, further confirming that soil brightness is not a major issue in the study area and that both indices can be used interchangeably.

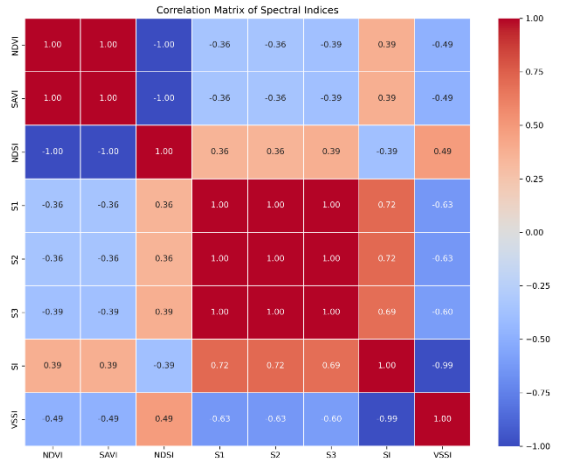

Figure 8 Correlation matrix showing relationships between vegetation, brightness, and composite salinity indices used to assess coastal salinization. Strong contrasts highlight complementary index behavior.

Salinity indices (S1, S2, S3) were also strongly intercorrelated (r = 1.00), demonstrating their coherence in capturing salt-affected bare soil across the landscape. S1 in particular exhibited the best class separation with moderate internal variation, supporting its utility as the most effective salinity index under local conditions. The composite salinity index S4, while positively correlated with S1 and S2 (r ≈ 0.72), showed a high internal standard deviation across land cover classes, indicating substantial within-class variability and reduced discriminatory power—likely due to its dependency on the NIR band, which introduces noise in low-vegetation areas.

The Vegetation-Soil Salinity Index (VSSI) exhibited a strong negative correlation with S4 (r = –0.99), further reinforcing its ability to distinguish between vegetated zones and salt-encrusted surfaces. Moderate to strong negative correlations between VSSI and the brightness-based indices (S1–S3, r ≈ –0.60) further highlight its effectiveness in detecting stressed vegetation under salinity pressure. Overall, the matrix emphasizes the complementary nature of vegetation and salinity indices and identifies S1 and VSSI as particularly effective for characterizing salinity impacts within the coastal Nile Delta setting.

Discussion

This study demonstrates that soil salinity from seawater intrusion measurably affects vegetation health and surface reflectance patterns across the Mansoura transect. While vegetation indices (NDVI, SAVI) successfully indicated areas of plant stress, their spatial coherence was limited, likely due to the confounding effects of irrigation and land management. In contrast, brightness-based indices (S1–S3) captured more consistent patterns of increasing soil salinity toward the coastal sabkha. Among these, S1 emerged as the most reliable indicator, offering strong mean separation between sabkha and vegetated zones and moderate internal variability, making it particularly effective under the local soil and moisture conditions. This is due to the dependence on the red and green bands which concentrate on soil brightness and identify the salt patches. Although the area has high moisture content, which was expected to hinder measurement using brightness-based indices, this index performed well due to the dark nature of the soil which allowed for more visibility and contrast of salt. S4, however, showed high standard deviation within each land cover class and poor class discrimination, in line with its known sensitivity to NIR noise.

The Vegetation–Soil Salinity Index (VSSI), by integrating both vegetation and brightness cues, revealed a strong inverse relationship with salinity indices, reinforcing its value in highlighting areas of vegetation loss due to salinity. While VSSI is not a direct salinity proxy, its high negative correlation with salinity indices makes it a powerful complementary tool in mixed-cover landscapes. Although these findings were based on a single Landsat image, they underscore that no single index suffices for brightness indices, especially S1, map salt accumulation in bare areas, while VSSI helps detect vegetative responses to salinity stress. This model is based solely on remotely sensed data without field validation due to lack of funding and equipment at the time of the study. We used previous work and previously

validated indices, some of which were used in the study area to validate our findings.

Conclusion and Recommendations

Soil salinity induced by seawater intrusion in the northeastern Nile Delta significantly reduces vegetation vigor and alters surface reflectance. Among the tested indicators, S1 provided the clearest separation between sabkha and vegetated zones, demonstrating its effectiveness in identifying salt-encrusted soils. The VSSI proved especially useful in mixed-cover areas, where it helped delineate zones of vegetation stress in response to underlying salinity. While NDVI and SAVI remain valid for vegetation monitoring, they are less reliable in areas affected by variable irrigation or sparse crop cover.

We recommend adopting a complementary index approach: using S1 for soil salinity detection and VSSI for early warning of salinity stress in crops. Routine monitoring with these indices, supported by targeted field surveys and conductivity data, can inform improved drainage, adaptive irrigation, and salt-tolerant crop strategies to sustain productivity in the face of rising salinization. for future work we suggest analyzing the salinity mapping in the area using different satellites imagery (e.g., Sentinel-2) to define the most efficient satellite and indices these results should be compared to field samples or geophysical studies to increase model certainty.

References:

Aeman, H., Shu, H., Abbas, S., Aisha, H., & Usman, M. (2023). Sinking delta: Quantifying the impacts of saltwater intrusion in the Indus Delta of Pakistan. Science of the Total Environment, 880. Https://doi.org/10.1016/j.scitotenv.2023.163356

ALSHRABSY, A. N., Kenawy, A. M., & Mohamed, E. F. (2024). Assessment of Irrigation Water Quality in the Reclaimed Lands in the North of Dakahlia Governorate. Journal of Soil Sciences and Agricultural Engineering, 15(3), 51–65. Https://doi.org/10.21608/JSSAE.2024.270005.1217

Armanuos, A. M., Gamal, M., Ibrahim, E., Negm, A., Takemura, J., Yoshimura, C., & Mahmod, W. E. (2022). Investigation of Seawater Intrusion in the Nile Delta Aquifer, Egypt. In Journal of Engineering Research (Vol. 6, Issue 1). ERJ.

Azabdaftari, A., & Sunar, F. (2016). SOIL SALINITY MAPPING USING MULTITEMPORAL LANDSAT DATA. The International Archives of the Photogrammetry, Remote Sensing and Spatial Information Sciences, XLI-B7, 3–9. Https://doi.org/10.5194/ISPRS-ARCHIVES-XLI-B7-3-2016

Bear, J. (1999). Seawater Intrusion in Coastal Aquifers — Concepts, Methods and Practices - Seawater intrusion in coastal aquifers : concepts, methods, and practices. In Theory and Applications of Transport in Porous Media: Vol. NA (Issue NA). Https://doi.org/10.1007/978-94-017-2969-7

Cao, X., Chen, W., Ge, X., Chen, X., Wang, J., & Ding, J. (2022). Multidimensional soil salinity data mining and evaluation from different satellites. Science of the Total Environment, 846. Https://doi.org/10.1016/j.scitotenv.2022.157416

Dehni, A., & Lounis, M. (2012). Remote sensing techniques for salt affected soil mapping: Application to the Oran region of Algeria. Procedia Engineering, 33, 188–198. Https://doi.org/10.1016/j.proeng.2012.01.1193

Douaoui, A. E. K., Nicolas, H., & Walter, C. (2006). Detecting salinity hazards within a semiarid context by means of combining soil and remote-sensing data. Geoderma, 134(1–2), 217–230. Https://doi.org/10.1016/j.geoderma.2005.10.009

El Nahry, A. H., Ibraheim, M. M., & El Baroudy, A. A. (2015). ASSESSMENT OF SOIL DEGRADATION IN THE NORTHERN PART OF NILE DELTA, EGYPT USING REMOTE SENSING AND GIS TECHNIQUES. Remote Sensing and Spatial Information Sciences. Https://doi.org/10.5194/isprsarchives-XL-7-W3-1461-2015

Huete, A. R. (1988). A Soil-Adjusted Vegetation Index (SAVI) 295. In REMOTE SENSING OF ENVIRONMENT (Vol. 25).

Khan, N. M., Rastoskuev, V. V, Shalina, E. V, & Sato, Y. (2001). Mapping Salt-affected Soils Using Remote Sensing Indicators-A Simple Approach With the Use of GIS IDRISI.

Mansour, M. M. A., & Mark, C. (2025). Land Productivity and Fertility Nexus Study in Dakahlia Governorate Using Gis and Remote Sensing. Journal of Soil Sciences and Agricultural Engineering, 16(3), 39–46. Https://doi.org/10.21608/JSSAE.2025.367377.1276

Montgomery, D. C. . (2013). Introduction to linear regression analysis. 163. Https://books.google.com/books/about/Introduction_to_Linear_Regression_Analys.html?Id=lsyirzh09oec

Nguyen, K. A., Liou, Y. A., Tran, H. P., Hoang, P. P., & Nguyen, T. H. (2020). Soil salinity assessment by using near-infrared channel and Vegetation Soil Salinity Index derived from Landsat 8 OLI data: a case study in the Tra Vinh Province, Mekong Delta, Vietnam. Progress in Earth and Planetary Science, 7(1), 1–16. Https://doi.org/10.1186/S40645-019-0311-0/FIGURES/11

Nofal, E. R., Amer, M. A., El-Didy, S. M., & Fekry, A. M. (2015). Delineation and modeling of seawater intrusion into the Nile Delta Aquifer: A new perspective. Water Science, 29(2), 156–166. Https://doi.org/10.1016/j.wsj.2015.11.003

Pennington, B. T., Sturt, F., Wilson, P., Rowland, J., & Brown, A. G. (2017). The fluvial evolution of the Holocene Nile Delta. Quaternary Science Reviews, 170, 212–231. Https://doi.org/10.1016/j.quascirev.2017.06.017

Youssef, Y. M., Gemail, K. S., Atia, H. M., & Mahdy, M. (2024). Insight into land cover dynamics and water challenges under anthropogenic and climatic changes in the eastern Nile Delta: Inference from remote sensing and GIS data. Science of the Total Environment, 913. Https://doi.org/10.1016/j.scitotenv.2023.169690

الملخص العربي

عنوان البحث: تحليل مقارن للمؤشرات الطيفية لتقييم تملّح السواحل في شمال شرق دلتا النيل، مصر

ريم علي النجار*[١]، أيمن طه[٢]، هاني شعبان[٢]، إيمان نوفل[٣]، حاتم أبو الخير[١]

[١]كلية العلوم، جامعة دمياط، ٣٤٥١٧، دمياط، مصر
[٢]المعهد القومي للبحوث الفلكية والجيوفيزيقية، ١١٧٢٢، حلوان، القاهرة، مصر
[٣]معهد بحوث المياه الجوفية، المركز القومي لبحوث المياه، ١٣٦٢١، القناطر الخيرية، مصر

يشكّل تملّح التربة الناتج عن تغلغل مياه البحر تهديدًا متزايدًا للزراعة في شمال شرق دلتا النيل، حيث تسهم المياه الجوفية الضحلة ونُظُم الريّ المكثفة في تراكم الأملاح على سطح التربة. تهدف هذه الدراسة إلى رسم خرائط لتوزيع الملوحة السطحية وتأثيرها على الغطاء النباتي على امتداد ٥٠ كيلومترًا من مدينة المنصورة الجديدة حتى مدينة المنصورة، باستخدام بيانات القمر الصناعي Landsat 8 OLI. تم تطبيق تصنيف غير موجّه باستخدام خوارزمية K-means لتحديد خمسة أنواع من استخدامات/أغطية الأرض (مياه، نباتات، أراضٍ جرداء، عمران، سبخة)، ما أتاح حساب ثمانية مؤشرات طيفية لكل فئة: NDVI، SAVI، NDSI، S1–S3، S4، VSSI. استُخدمت الإحصاءات النطاقية لتحليل توزيعات المؤشرات، بينما استخدم الانحدار الخطي لتقييم الاتجاهات المكانية للمؤشرات وفقًا للمسافة من الخط الساحلي. أظهرت مؤشرات الغطاء النباتي NDVI، SAVI قدرة على تمييز الإجهاد النباتي، لكنها لم تُظهر تدرجات ساحلية واضحة ($\beta_1 \approx -1.8 \times 10^{-6}$ م$^{-1}$؛ $R^2 \approx 0$)، مما يعكس فعالية الري المحلي في التخفيف من آثار الملوحة. أما المؤشرات المعتمدة على السطوع ومؤشر NDSI، فقد رصدت تراكُم القشور الملحية بوضوح، حيث ازدادت القيم المتوسطة لمؤشرات S1–S3 من الأراضي الزراعية (١٣,٢٢٢–١٤,٩٧٢) إلى مناطق السبخة (١٩,١٢٢–٢٠,٠٨٠) مع وجود ميل إيجابي طفيف نحو الساحل مثلًا: β_1 لمؤشر S1 = 0.1255 م$^{-1}$؛ ($R^2 < 0.003$). وقد أظهر المؤشر الهجين VSSI أعلى قدرة على التمييز بين المناطق النباتية والمناطق المتضررة من التملّح (متوسط (–٧٩,١٦٣) مقابل)–١٢٥,٦١ (تُظهر هذه النتائج تفاوت حساسية المؤشرات الطيفية تجاه الملوحة والإجهاد النباتي، مما يتيح مراقبة ملوحة التربة بكفاءة وتكلفة منخفضة، وتوجيه التحاليل والمسوح التفصيلية فقط عند الضرورة.